Shapes of Buoyant and Nonbuoyant Laminar Jet Diffusion Flames

P. B. SUNDERLAND*
National Research Council, Cleveland, OH 44135

B. J. MENDELSON
Department of Mechanical and Aerospace Engineering, Princeton University, Princeton, NJ 08544

Z.-G. YUAN
National Center for Microgravity Research, Cleveland, OH 44135

D. L. URBAN
NASA Lewis Research Center, Cleveland, OH 44135

Flame shapes were measured for buoyant and nonbuoyant laminar gas jet diffusion flames burning, methane, ethane, and propane in quiescent air. Test conditions involved burner diameters of 0.19–5.5 mm, ambient pressures of 0.25–2 atm, and fuel flowrates of 0.04–4.6 mg/s. Care was taken to minimize interference from soot emissions and from ignition disturbances. Microgravity conditions were obtained in the 2.2-s drop tower at the NASA Lewis Research Center. Normalized lengths of both buoyant and nonbuoyant flames were proportional to source Reynolds number, but the nonbuoyant flames were 40% longer on average. Normalized widths of the nonbuoyant flames were constant for $Re \geq 100$, whereas buoyant flame widths scaled with source Froude number. Several nonbuoyant flame models are evaluated with the present shape data.

NOMENCLATURE

D	mass diffusivity
d	burner inside diameter
Fr	source Froude number: $Fr = u^2/gd$
g	acceleration of gravity
L	stoichiometric or luminous flame length
$\dot{m}$	fuel mass flowrate
p	ambient pressure
Re	source Reynolds number: $\mathrm{Re} = \rho u d/\mu = 4\dot{m}/\pi\mu d$
St	source Stokes number: $St = Fr/Re$
T	temperature
t	time after ignition
t_{ch}	characteristic time
u	area-averaged fuel source velocity: $u = 4\,\dot{m}/\pi\rho d^2$
w	maximum stoichiometric or luminous flame width
z	axial distance
μ	source fuel dynamic viscosity at 298 K
ρ	source fuel density at p and 298 K

*Corresponding author. NASA Lewis Research Center, M.S. 500-115, 21000 Brookpark Rd., Cleveland, OH 44135. E-mail: pbs@einstein.lerc.nasa.gov

0010-2180/99/$19.00
PII S0010-2180(98)00045-5

INTRODUCTION

Laminar gas jet diffusion flames are fundamental to combustion. Their study has contributed to myriad advances in combustion science, including the development of theoretical, computational, and diagnostic combustion tools. Laminar jet flames are pertinent to the turbulent flames of more practical interest via the laminar flamelet concept [1, 2].

Flame shape is an important characteristic of laminar diffusion flames that has been modeled and measured using numerous techniques. Shape can be profoundly affected by gravity; thus observations of shapes at varying gravitational level are especially useful in the evaluation of models. Until now there has been no robust set of measurements of microgravity gas jet stoichiometric flame shapes and, in contrast to numerous correlations of flame length, empirical correlations of widths of laminar gas jet flames are conspicuously absent from the literature.

The proportionality between laminar jet flame length and fuel mass flowrate, and the independence of length from pressure and

COMBUSTION AND FLAME 116:376–386 (1999)

Published by Elsevier Science Inc.

burner diameter, is a classical relation of combustion science. This is commonly expressed as $L/d \propto Re$ or, equivalently, $L \propto \dot{m}$. Jost [3] obtained this by equating convection time, L/u, with diffusion time, $d^2/8D$. Most laminar jet flame models predict the same behavior, particularly when axial diffusion and gravity are neglected [4–9]. When gravity is included, Jost's analysis incorrectly predicts longer flames. Roper's improved analysis [10] showed that competing effects of residence time and concentration gradients result in flame lengths that are independent of gravitational level for circular burners. Others also obtained $L \propto \dot{m}$ in buoyant flames by using scaling arguments [11, 12] and numerical solutions of the parabolic [13, 14] and elliptic [15] governing equations. Deviations from $L \propto \dot{m}$ in buoyant flames have been suggested [9, 16].

There are two recurrent width predictions, one each for nonbuoyant and buoyant flames. For nonbuoyant flames, many models predict $w \propto d$ regardless of pressure or flowrate [4, 6, 8]. In the spirit of Jost, this results from equating convection time (L/u and thus $\dot{m}/u$) with a width-related diffusion time ($w^2/4D$). For buoyant flames the common prediction is $w/d \propto St^{0.25}$. This results from a Jost-type analysis, and from more advanced models [10–12], when buoyant velocity is scaled as $u \propto (gz)^{1/2}$.

There has been abundant experimental confirmation of the relation $L \propto \dot{m}$ in buoyant flames [12, 14, 15, 17] and in nonbuoyant flames [2, 18–20], which were found to be longer. To date, no experimental study has presented correlations of either buoyant or nonbuoyant laminar jet flame widths; such correlations would allow more complete testing of analytical models. An additional shortcoming of previous experimental work is the reporting of luminous flame shapes instead of the stoichiometric shapes that most models predict. Soot emissions can obscure the stoichiometric flame sheet; this accounts for luminous lengths exceeding stoichiometric lengths by 10–60% [15, 21]. Many studies of buoyant flame shapes attempted to correct for this [12, 14, 15, 17], whereas previous studies of nonbuoyant hydrocarbon flame shapes did not [2, 18–20, 22, 23]. They reported that microgravity flames were longer and wider, but could not rule out the possibility that this was an artifact of soot emissions in their relatively sooty flames. Previous studies of nonbuoyant flame shapes were conducted in drop towers, but long-duration (space-based) measurements of these shapes have recently been completed by Lin et al. [24].

In light of the above, the objectives of the present work were: obtain stoichiometric flame-shape measurements of buoyant and nonbuoyant laminar gas jet diffusion flames; consider various fuels, burner sizes, pressures, and flowrates; correlate the lengths and widths of buoyant and nonbuoyant flames; and compare these correlations with published models. Flame images were obtained for methane, ethane, and propane flames burning in quiescent air. Soot concentrations were minimized by selecting conditions at low $\dot{m}$ and p; this facilitated identification of the stoichiometric flame sheet. Flame shapes were determined for 70 nonbuoyant and 231 buoyant flames.

EXPERIMENTAL METHODS

The experiments were conducted in a windowed pressure vessel supported by a fuel-delivery system, an ignitor, a color CCD camera, a microprocessor controller, and lead-acid batteries. The burners were straight stainless steel tubes with beveled outside edges and inside diameters of 0.19, 0.42, 0.85, 1.70, 3.25, and 5.54 mm; all burners had length-to-diameter ratios of at least 40 to ensure fully developed laminar discharge. The fuel jets issued vertically upward on the axis of the cylindrical chamber, whose diameter, length, and volume were 25 cm, 53 cm, and 27 liters, respectively. Microgravity conditions were obtained in the NASA Lewis 2.2-s drop tower.

On-board methane, ethane, and propane (purities 99.99%, 99.9%, and 99.9%, respectively) were stored in a 75-ml bottle and delivered to the burner via a pressure regulator, a solenoid valve, a critical-flow orifice, a mass-flow meter, and a second solenoid valve. Orifice diameters (0.03–0.07 mm) were selected to ensure choked flow. Fuel flowrates were determined using the mass-flow meter, which was calibrated for each fuel using a bubble meter. Ambient air was used as the oxidizer for conditions at or below 1 atm;

TABLE 1

Test Flame Summary

	d (mm)	p (bar)	$\dot{m}$ (mg/s)	u (m/s)	Re (−)	Fr (−)	L (mm)	w (mm)	Flame Count
Nonbuoyant flames	0.42–3.3	0.25–0.98	0.13–2.3	0.02–26	10–740		2–60	4–36	70
Buoyant flames	0.19–5.5	0.25–1.97	0.04–4.6	0.001–19	5–1,020	0.001–86,000	1–84	1–15	231

a mixture of 21.1% O_2 (by volume), balance N_2 was used for the 2-atm flames.

Microgravity laminar jet flames are sensitive to hydrodynamic disturbances such as those caused by prerelease ignition, articulating ignitors, and initial deflagrations. To avoid these, the present nonbuoyant flames were ignited after release into microgravity using spring-loaded hot wires (Kanthal A, with lengths of 12 mm and diameters of 0.36 mm) mounted in tension 3 mm above the burners. The ignitors were energized with 28 VDC, whereby they quickly glowed, ruptured, and retracted with minimal wakes. Another novel feature of the present hardware was the serial pair of solenoid valves which facilitated smooth ignition via optimization of the volume of the initial fuel discharge.

The flames were imaged through the chamber window using a color CCD camera (Panasonic WV-CL352). Fixed-iris lenses were used, with focal lengths (16–50 mm) selected according to flame size, and f numbers (1.4–6) chosen according to flame luminosity. Video signals were carried via fiber-optic cable to a stationary S-VHS video recorder. Spatial resolution in the video images was 0.1 mm or better.

We endeavored to measure stoichiometric, as opposed to luminous, flame shapes. Mitchell et al. [15] observed blue flame emissions (which arise from CH and CO_2) to coincide with stoichiometric conditions. Thus the stoichiometric dimensions reported here were determined from contours of peak blue luminosity. For flames containing soot, an additional camera equipped with a CH-line filter (430 ± 5 nm) facilitated stoichiometric flame sheet observation. No correction has been made for line-of-sight integration errors.

We sought the widest possible range of test conditions, as summarized in Table 1. Low pressures were emphasized to minimize soot interference. The lower limit of Re for both buoyant and nonbuoyant flames was governed by the onset of crescent-shaped flames, whose maximum widths were at their bases. The upper limit of Re was demarcated by lifted, excessively sooty, or (in normal gravity) flickering flames. All the flames reported here were attached, laminar, and nonflickering.

Uncertainties (at the 95% confidence level) are estimated to be 5% for measurements of flowrates, lengths of soot-free flames, and widths. Uncertainties of flame lengths at the highest flowrates and pressures were 10% due to soot interference. Unsteady effects in the microgravity flames augment these estimates by 5%, as discussed below.

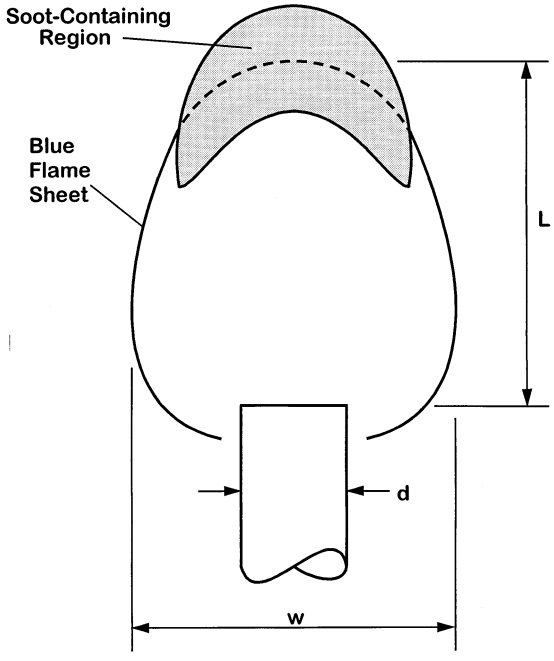

Fig. 1. Sketch of a typical soot-containing laminar jet diffusion flame.

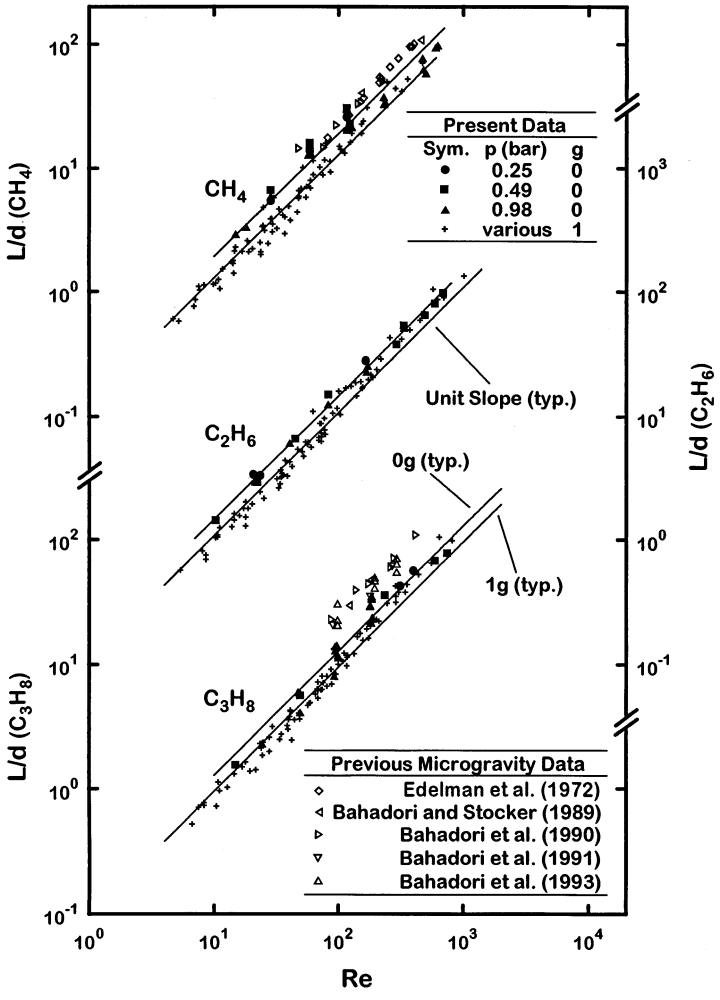

Fig. 4. Stoichiometric lengths of buoyant and nonbuoyant flames. Correlations shown are given in Table 2. Previous data is from Refs. 18–20, 22, 23.

RESULTS AND DISCUSSION

Flame Appearance

Figure 1 is a sketch of the typical appearance and dimensions of the present flames. L is height above the burner lip at which the stoichiometric flame sheet crosses the axis and w is the stoichiometric width of the flame at its broadest section. Figure 2 shows a pair of captured video images of low-*Re* ethane flames 2 s after ignition. Other than gravitational level, the conditions for these two flames are identical, allowing a side-by-side comparison of buoyant and nonbuoyant flames. The buoyant flame has familiar features: a well-defined blue flame sheet, a dim blue interior, and a small yellow soot tongue overlapping the flame tip. The corresponding nonbuoyant flame has a much larger flame sheet and contains no soot. Its relative sphericity and its extension below the burner lip demonstrate the dominance of diffusion over convection at these conditions. Figure 3 shows a pair of high-*Re* ethane flames, where again the lens and camera settings are matched and the only difference is gravitational level. These images demonstrate the diminished effect of buoyancy on the shapes of high-*Re*, momentum-dominated laminar jet flames.

Many of the present flames contained no visible soot, permitting precise determinations of stoichiometric lengths and widths. Yellow luminosity, attributed to soot, increased with fuel carbon content, pressure, and flowrate, but no flame emitted soot; furthermore, the nonbuoyant flames contained less soot than their long-duration counterparts [2, 25]. Soot emis-

TABLE 2

Determinations of $L/(dRe)$

	CH_4	C_2H_6	C_3H_8
Present nonbuoyant[a]	0.192 ± 0.018	0.146 ± 0.007	0.128 ± 0.012
Present buoyant[a]	0.129 ± 0.006	0.108 ± 0.005	0.095 ± 0.004
Mahalingam et al.[b] [8]	0.199	0.172	0.153
Roper[c] [10]	0.178	0.137	0.116
Klajn and Oppenheim[d] [6]	0.149	0.138	0.134

[a] Geometric mean ± symmetrized 95% confidence interval.
[b] Predicated on the density and the fuel–N_2 diffusivity of an equimolar mixture of fuel and N_2 at 1500 K.
[c] Adopting Roper's characteristic temperature of 1500 K and his reference diffusivity of 20 mm^2/s at 1.01 bar and 298 K.
[d] Assuming adiabatic flame temperatures of 2226, 2260, and 2267 K for methane, ethane, and propane, and incorporating the additional factor of $3^{-0.5}$ [6].

sions had no impact on width measurements (see Figs. 1–3), but occasionally impeded determinations of stoichiometric lengths, for which tests a second video camera equipped with a CH-line filter proved beneficial.

The short duration of the present microgravity tests required consideration of flame-shape steadiness. This concern was addressed by minimizing ignition disturbances and by considering the time-extrapolation analysis of Tittmann et al. [26], $L(t)/L(\infty) = e^{-t_{ch}/t}$, and the corresponding analysis of widths, where t_{ch} is determined experimentally for each test. In contrast, to the technique of Ref. 26, the present nonbuoyant flames were ignited after release and quickly approached steady shapes. Our extrapolation analysis indicates that the present flames attained lengths and widths which were within 5% of their steady-state values. Consequently, the dimensions we report herein correspond to end-of-test conditions.

Flame Lengths

Figure 4 shows measured stoichiometric lengths of the present buoyant and nonbuoyant flames, normalized by burner diameter and plotted versus *Re*. This choice of axes follows a long tradition in the literature [5, 6, 9, 15, 18–20]. Least-squares fits through the present buoyant and nonbuoyant lengths have slopes averaging 1.09 and 0.98, respectively, but in accordance with theory [3–15] we instead correlate the data with unity slopes (reflecting $L \propto \dot{m}$), the coefficients for which are given in Table 2. We found no statistically significant dependence of L on either d or p in nonbuoyant flames; we found normal-gravity lengths to increase slightly with reductions in d and p, in concurrence with Ref. 27 observations. Also shown in Fig. 4 are lengths of previous microgravity methane and propane flames [18–20, 22, 23], nearly all of which involved atmospheric-pressure conditions. These also can be approximated with unity-slope fits. Because these are luminous lengths of relatively sooty flames, their fits average 49% longer than the present nonbuoyant correlations.

The present nonbuoyant flames are, on average, 40% longer than buoyant flames at corresponding *Re*. The decrease of *luminous* flame length with increasing gravitational level has been observed before in microgravity flames [2, 18–20, 22, 23 and references therein] and in centrifuge flames [16], but the present study is the first to report such behavior for *stoichiometric* lengths of hydrocarbon flames. The difference between buoyant and nonbuoyant flame lengths decreases as *Re* increases. This occurs since in buoyant flames *Fr* (the ratio of momentum to buoyancy forces) generally increases with *Re*. Present flame shapes (e.g., Figs. 3 and 4) support the suggestion of Davis et al. [28] that at sufficiently large *Fr*, nonflickering normal-gravity laminar jet flames approach nonbuoyant behavior.

Many explanations have been proposed for the increased lengths of nonbuoyant laminar jet flames. Increased axial diffusion may be a factor [19, 29]. Some instead blame decreased oxidizer entrainment [9, 13, 16], which is not captured by analytical models that neglect radial convection. Roper's model includes radial convection and nevertheless predicts length to be independent

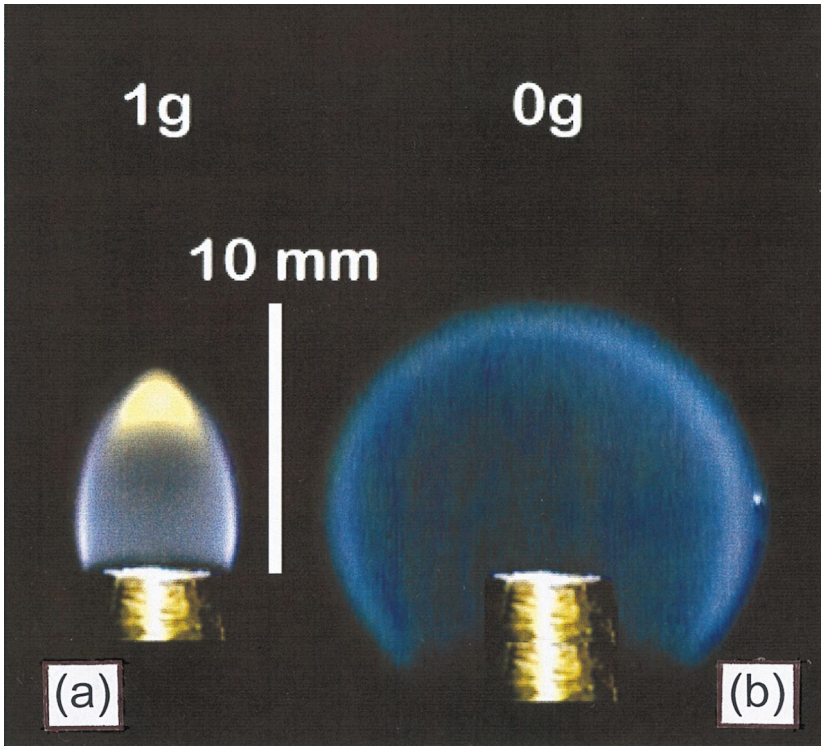

Fig. 2. Images of low-*Re* ethane flames with $d = 3.3$ mm, $p = 0.98$ bar, and $Re = 21$, with burners enhanced. (a) Buoyant, $Fr = 0.08$. (b) Nonbuoyant.

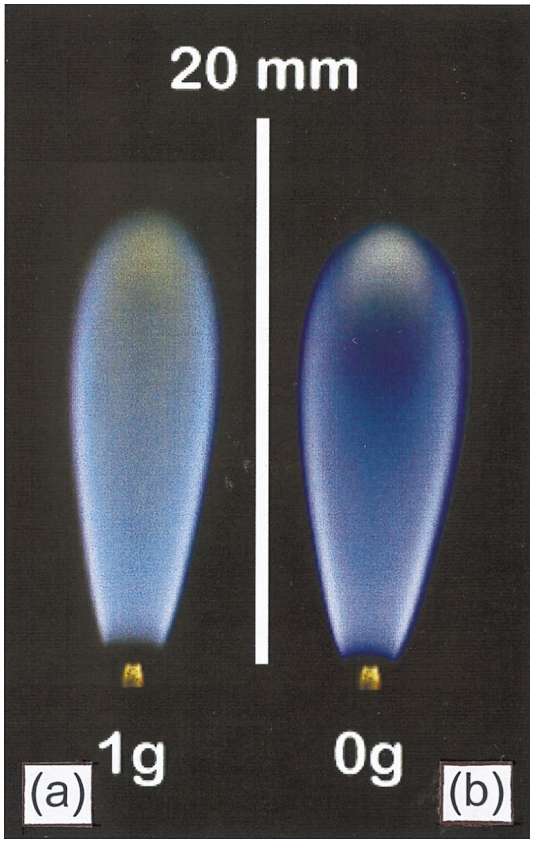

Fig. 3. Images of high-*Re* ethane flames with $d = 0.42$ mm, $p = 0.49$ bar, and $Re = 291$, with burners enhanced. (a) Buoyant, $Fr = 28{,}200$. (b) Nonbuoyant.

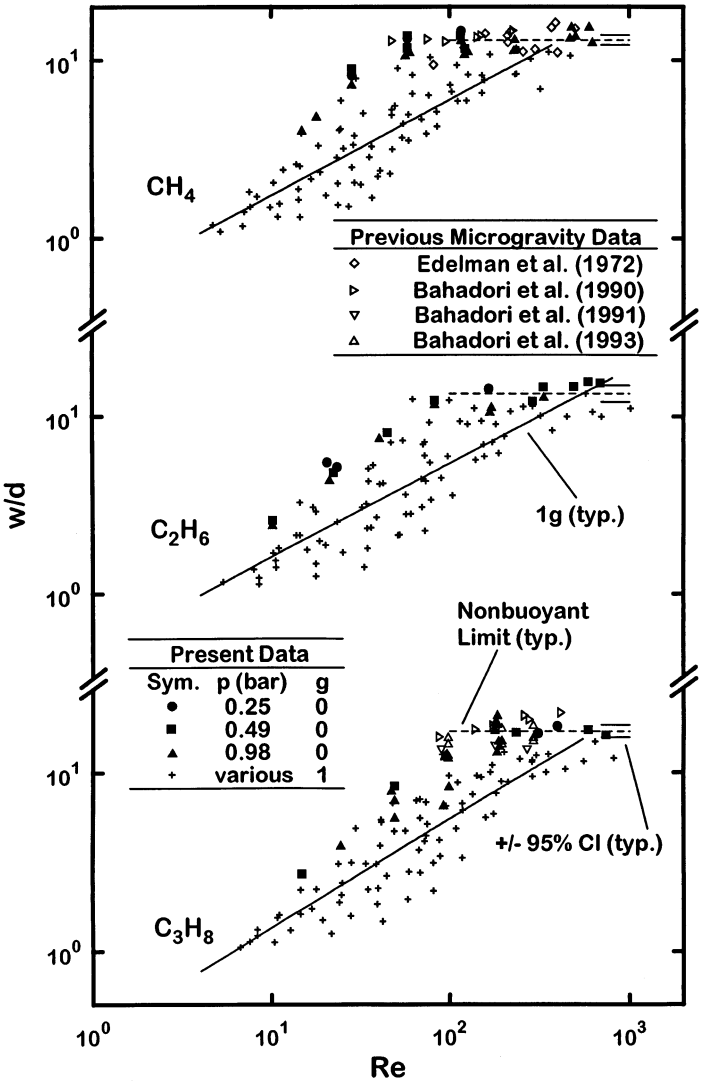

Fig. 5. Stoichiometric widths of buoyant and nonbuoyant flames. Nonbuoyant limit correlations are given in Table 3. Previous data is from Refs. 18–20, 23.

of gravitational level [10]; he suggests the observed difference could be due to Kelvin-Helmholtz instabilities [30] outside buoyant laminar jet flames. Although Roper himself did not mention this, we find plausible his model's indication that the increased lengths of nonbuoyant flames could arise from reduced mass diffusivities associated with reduced temperatures. Roper quantified this as $L \propto T_f^{-0.67}$, where T_f is the characteristic temperature controlling mass diffusion. The Roper model (with $D = 20$ mm^2/s at 1.01 bar and 298 K) best matches lengths of the present buoyant and nonbuoyant flames when T_f is 2190 and 1330 K respectively. (Roper invoked a temperature of 1500 K in matching the luminosity lengths of normal-gravity flames.) These temperatures cannot be validated since measurements to date have not resolved the peak temperatures in microgravity laminar jet flames. Numerical models differ in their predictions of these temperatures. Bahadori et al. [31] predicted a dramatic influence of gravity on the peak temperatures at the broadest height of a propane flame: 2200 and 1400 K for normal- and reduced-gravity, respectively. Kaplan et al. [32] predicted a smaller difference (in ethylene flames): 2050 and 2000 K, respectively. Whether temperature explains the variation of length with gravitational level remains an open question.

Several models predict length scaling of the

TABLE 3

Determinations of w/d

	CH_4	C_2H_6	C_3H_8
Present nonbuoyant limit[a]	13.0 ± 0.8	13.4 ± 1.5	17.1 ± 1.4
Mahalingam et al. [8]	2.59	2.51	2.48
Roper[b] [10]	4.42	5.73	6.78
Klajn and Oppenheim[c] [6]	15.6	14.7	14.3

[a] Geometric mean ± symmetrized 95% confidence interval.

[b] Following the numerical quadrature of [34], assuming uniform velocity and adopting Roper's characteristic temperature of 1500 K.

[c] Assuming adiabatic flame temperatures of 2226, 2260, and 2267 K for methane, ethane, and propane, and incorporating the additional factor of $3^{-0.5}$ [6].

form $L/d \propto (Re^2Fr)^{1/3}$ in the pure buoyant regime under the assumption of constant w/d (Refs. 9 and 16 and references therein). In an experimental study of diffusion flame lengths in elevated gravity, Altenkirch et al. [16] plotted $L/d(Re^2Fr)^{1/3}$ versus Fr. Their data provided only weak support for $L/d \propto (Re^2Fr)^{1/3}$ at low Fr; they correlated the bulk of their data empirically with a slope of $-1/4$. Villermaux and Durox [9] analyzed the same data with a model they claimed predicts a slope of $-1/6$ at large Fr, but this prediction requires constant d, p, and g since their actual nonbuoyant prediction is $L/d \propto Re$. When plotted on the axes of Ref. 16, our normal-gravity data is best correlated with a slope of -0.23. The present data does not level off at low Fr even though our Froude numbers extended 2–3 orders of magnitude lower than those reported for corresponding fuels in [16]. In light of past use of Fr in correlating lengths of buoyant flames, we considered more general correlations of the form $L/d \propto Re^aFr^b$. The present normal-gravity flames are best correlated with $a = 0.93$ and $b = 0.05$, which is strong empirical support for $L/d \propto Re$ in buoyant flames.

Flame Widths

Motivated by the above analysis of flame lengths, correlations between normalized stoichiometric flame widths and Re were considered, as shown in Fig. 5. The previous nonbuoyant luminous widths shown in Fig. 5 [18–20, 23] agree with present nonbuoyant measurements since luminous and stoichiometric widths typically match (see Figs. 1–3). Similar to observations of flame lengths, the present nonbuoyant flames were wider than buoyant flames at corresponding Re and the difference diminished as Re increased. We attribute the width difference to radial convection: flow in nonbuoyant flames is radially outward, which moves the stoichiometric contour away from the centerline; in buoyant flames radial convection is mostly inward, thus having the opposite effect [2, 13, 25]. The convergence of buoyant and nonbuoyant widths at high Re results from diminished effects of buoyancy relative to momentum in normal-gravity laminar jet flames at high Re (i.e., at high Fr) [28].

Nonbuoyant laminar jet flame widths exhibit different behaviors in the low- and high-Re regimes. At low Re, nonbuoyant flames tend toward sphericity (see Fig. 2b) and thus w/d increases with Re similar to the behavior of flame lengths. However, for source Reynolds numbers exceeding 100, flames become elongated and normalized widths remain fixed regardless of Re. Support for constant normalized widths comes from models that neglect buoyancy and that assume boundary-layer (high-Re) behavior [4, 6, 8, 10]. We determined nonbuoyant width limits by excluding flames with $Re < 100$ and by evaluating geometric averages of the remaining normalized widths; those limits are shown as horizontal fits in Fig. 5 and are enumerated in Table 3.

Following the failure of Re to correlate the widths of buoyant laminar jet flames, regressions of the form $w/d \propto Fr^aRe^b$ were considered. As discussed above, several theories predict $a = -b = 0.25$, or $w/d \propto St^{0.25}$ [10–12]. The present data rejects, at the 5% significance

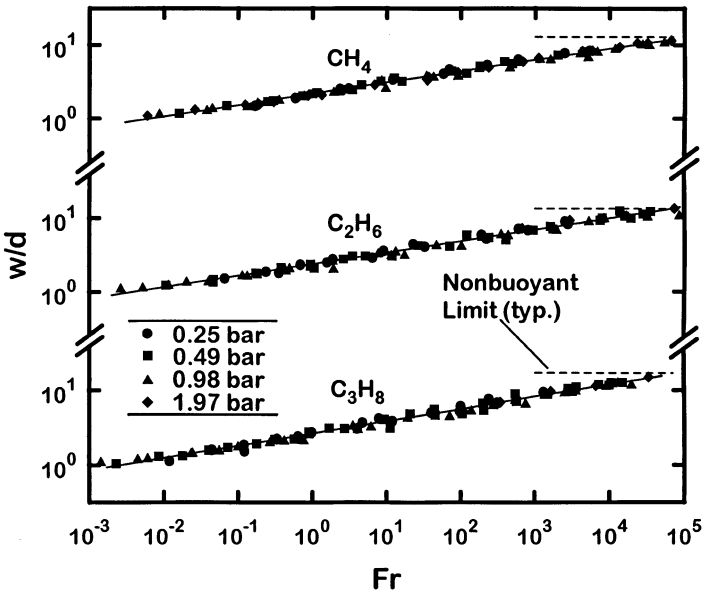

Fig. 6. Stoichiometric widths of buoyant flames. Correlations shown are: CH_4: $w/d = 2.17Fr^{0.154}$; C_2H_6: $w/d = 2.38Fr^{0.155}$; and C_3H_8: $w/d = 2.66Fr^{0.163}$.

level, the null hypotheses $a = 0.25$ and $b = -0.25$, but cannot reject, at the same level, the null hypothesis $b = 0$. Accordingly, we plot w/d versus Fr for the present buoyant flames in Fig. 6. The slopes average 0.16 and the correlations are remarkable, with R^2 correlation coefficients exceeding 0.98. At the highest Fr, the normalized widths of the present buoyant flames approach the nonbuoyant width limits, shown as dotted lines in Fig. 6. At such high Fr, normal-gravity laminar jet flames become essentially nonbuoyant. Further increases in Fr should cause normal-gravity flame widths to level off at the nonbuoyant width limits, but we were unable to demonstrate this due to flame lift-off.

Never before have laminar jet flame widths been correlated with Fr, although Fr has previously appeared in length correlations of both laminar [9, 16] and turbulent [33] jet diffusion flames. Some additional remarks concerning Fig. 6 are thus provided. The dependence of w/d on d in the correlations of Fig. 6 is small, but is statistically supported by our measurements. Although the correlations include g, we have no evidence they are valid at different gravity levels. However, a slight decrease of widths with increasing gravity, suggested by Fig. 6, was observed in centrifuge flames [16] and is predicted by relations of the form $w/d \propto St^{0.25}$ [10–12]. Furthermore, Davis et al. [28] showed that Froude number is the appropriate scaling parameter for gravitational variations in laminar jet diffusion flames.

Nonbuoyant-Model Evaluation

As mentioned at the outset, one motivation for this work was an empirical evaluation of existing flame models. To this end we consider three analytical models [6, 8, 10] that predict shape contours of laminar gas jet diffusion flames. Two of these [8, 10] assume a coflowing ambient, while the third [6] assumes a quiescent ambient. The three models assume boundary-layer (high-Re) behavior and only one [10] allows buoyancy. Accordingly, the comparisons are based on predicted and measured lengths and high-Re widths (width limits) of nonbuoyant flames.

We consider first the Burke-Schumann model [4], as approximated by Mahalingam et al. [8] in the limit of infinite coflow tube radius. Its predicted lengths depend on ρD, which is assumed constant. When ρ and D pertain to an equimolar mixture of fuel and N_2 at 1500 K, predicted lengths are in reasonable agreement with present nonbuoyant observations, as shown in Table 2. The Burke-Schumann width predictions depend only on stoichiometry. Those predictions, shown in Table 3, are less than 20% of

measured widths as a result of the model's neglect of radial convection.

Roper [10] extended Burke and Schumann's analysis to allow radial convection and axial variations of velocity. For length predictions his model requires specifications of D and T. When Roper's property values are invoked, predicted and measured nonbuoyant lengths agree reasonably (Table 2). Recall that Roper's characteristic temperature of 1500 K falls between the temperatures that best match our buoyant and nonbuoyant flame length correlations. Roper's width predictions depend on specifications of axial velocity and temperature, which are used to model entrainment and thermal expansion. Under the assumption of constant axial velocity, predicted widths fall short of nonbuoyant-flame observations (Table 3). The agreement with nonbuoyant flame widths could be improved by specifying more realistic velocities that decay with axial distance.

Finally, we examine the analysis of Klajn and Oppenheim [6], which includes radial convection and the centerline velocity decay of nonbuoyant flames. This model's predictions of L/dRe and w/d, shown in Tables 2 and 3, depend only on stoichiometry and assumed adiabatic flame temperature. Like the other models [8, 10] the Klajn and Oppenheim model reveals the relative ease of accurate flame length predictions. Because this model includes centerline velocity decay, it better predicts the widths of high-Re nonbuoyant flames than do the other two models. The Klajn and Oppenheim model has a quiescent ambient, which also may aid its agreement with these widths. This model incorrectly predicts the observed variation of width with fuel type for the present fuels but nevertheless better approximates the present flame shapes than do the other models considered here.

CONCLUSIONS

Shapes of buoyant and nonbuoyant light hydrocarbon laminar jet diffusion flames were measured, considering variations in burner diameter, pressure, and fuel mass flowrate, and avoiding interference from soot emissions. The major findings were as follows:

- Buoyant and nonbuoyant stoichiometric flame lengths are proportional to fuel mass flowrate and independent of pressure and burner diameter; i.e., $L/d \propto Re$. Nonbuoyant flames are 40% longer on average, although the difference decreases as Re increases.
- Buoyancy reduces flame widths via effects of radial convection. Normalized widths of nonbuoyant flames approach a fuel-specific constant value as Re increases.
- Buoyant flame widths correlate with Fr and, for large Fr, approach the nonbuoyant limit.
- Three established models furnish reasonable flame length predictions. Only one of these [6] accurately predicts the widths of nonbuoyant flames. No existing model predicts the observed correlation of buoyant flame widths with Fr.

This work was supported under a NASA/NRC postdoctoral fellowship and was performed at NASA Lewis. We gratefully acknowledge the generous assistance of H. D. Ross, G. M. Faeth, and I. S. Wichman.

REFERENCES

1. Bilger, R. W., *Combust. Flame* 30:277 (1977).
2. Urban, D. L., Yuan, Z.-G., Sunderland, P. B., Linteris, G. T., Voss, J. E., Lin, K.-C., Dai, Z., Sun, K., and Faeth, G. M., *AIAA J.* (in press).
3. Jost, W., *Explosion and Combustion Processes in Gases*, McGraw-Hill, New York, 1946, p. 212.
4. Burke, S. P., and Schumann, T. E. W., *Ind. Eng. Chem.* 20:998 (1928).
5. Kanury, A. M., *Introduction to Combustion Phenomena*, Gordon and Breach, Amsterdam, 1975, p. 241.
6. Klajn, M., and Oppenheim, A. K., *Nineteenth Symposium (International) on Combustion*, The Combustion Institute, Pittsburgh, 1982, p. 223.
7. Kuo, K. K., *Principles of Combustion*, Wiley, New York, 1986, p. 366.
8. Mahalingam, S., Ferziger, J. H., and Cantwell, B. J., *Combust. Flame* 82:231 (1990).
9. Villermaux, E., and Durox, D., *Combust. Sci. Technol.* 84:279 (1992).
10. Roper, F. G., *Combust. Flame* 29:219 (1977).
11. Markstein, G. H., and De Ris, J., *Twentieth Symposium (International) on Combustion*, The Combustion Institute, Pittsburgh, 1984, p. 1637.
12. Saito, K., Williams, F. A., and Gordon, A. S., *Combust. Sci. Technol.* 47:117 (1986).
13. Miller, J. A., and Kee, R. J., *J. Phys. Chem.* 81:2534 (1977).

14. Li, S. C., Gordon, A. S., and Williams, F. A., *Combust. Sci. Technol*. 104:75 (1995).
15. Mitchell, R. E., Sarofim, A. F., and Clomburg, L. A., *Combust. Flame* 37:227 (1980).
16. Altenkirch, R. A., Eichhorn, R., Hsu, N. N., Brancic, A. B., and Cevallos, N. E., *Sixteenth Symposium (International) on Combustion*, The Combustion Institute, Pittsburgh, 1976, p. 1165.
17. Roper, F. G., Smith, C., and Cunningham, A. C., *Combust. Flame* 29:227 (1977).
18. Edelman, R. B., Fortune, O. F., Weilerstein, G., Cochran, T. H., and Haggard, J. B., *Fourteenth Symposium (International) on Combustion*, The Combustion Institute, Pittsburgh, 1972, p. 399.
19. Bahadori, M. Y., Edelman, R. B., Stocker, D. P., and Olson, S. L., *AIAA J*. 28:236 (1990).
20. Bahadori, M. Y., Stocker, D. P., Vaughan, D. F., Zhou, L., and Edelman, R. B., in *Modern Developments in Energy, Combustion and Spectroscopy*, (F. A. Williams et al., Eds.), Pergamon Press, Oxford 1993, p. 49.
21. Gomez, A., Sidebotham, G., and Glassman, I., *Combust. Flame* 58:45 (1984).
22. Bahadori, M. Y., and Stocker, D. P. (1989). Combustion Institute Eastern States Meeting, Paper 71.
23. Bahadori, M. Y., Edelman, R. B., Sotos, R. G., and Stocker D. P. (1991). AIAA Paper 91-0719.
24. Lin, K.-C., Faeth, G. M., Sunderland, P. B., Urban, D. L., and Yuan, Z.-G., *Combust. Flame* 116:415–431 (1998).
25. Sunderland, P. B., Mortazavi, S., Faeth, G. M., and Urban, D. L., *Combust. Flame* 96:97 (1994).
26. Tittmann, K., Sitzki, L., Bringezu, D., Rau, H., and Grabski, R., *Micrograv. Sci. Tech*. 9:40 (1996).
27. Yuan, T., Durox, D., and Villermaux, E., *Combust. Sci. Technol*. 92:69 (1993).
28. Davis, R. W., Moore, E. F., Santoro, R. J., and Ness, J. R., *Combust. Sci. Technol*. 73:625 (1990).
29. Chung, S. H., and Law, C. K., *Combust. Sci. Technol*. 37:21 (1984).
30. Wohl, K., Gazley, C., and Kapp, N., *Third Symposium on Combustion, Flame and Explosion Phenomena*, Williams & Wilkins, Baltimore, 1949, p. 288.
31. Bahadori, M. Y., Small, J. F., Hegde, U. G., and Stocker, D. P., (1996). Paper 96F-116, Combustion Institute Fall Western States Meeting.
32. Kaplan, C. R., Oran, E. S., Kailasanath, K., and Ross, H. D., *Twenty-Sixth Symposium (International) on Combustion*, The Combustion Institute, Pittsburgh, 1996, p. 1301.
33. Delichatsios, M. A., *Combust. Flame* 92:349 (1993).
34. Sunderland, P. B., Yuan, Z.-G., and Urban, D. L., *Proceedings of the Combustion Institute Central States Meeting*, 1997, p. 55.

Received 7 December 1997; accepted 1 April 1998